Gondwana Research 96 (2021) 76–88

Contents lists available at ScienceDirect

Gondwana Research

journal homepage: www.elsevier.com/locate/gr

Detrital zircon U-Pb-Hf isotopes from the Yanliao intracontinental rift sediments: Implications for multiple phases of Neoarchean-Paleoproterozoic juvenile crustal growth in the North China Craton

Xiaoping Liu [a,b], Huichuan Liu [a,b,*], Pin Gao [c], Wenqi Li [a,b], Huan Liu [a,b], Jiakai Hou [a,b]

[a] State Key Laboratory of Petroleum Resources and Prospecting, China University of Petroleum (Beijing), Beijing 102249, China
[b] College of Geosciences, China University of Petroleum (Beijing), Beijing 102249, China
[c] School of Earth Sciences and Resources, China University of Geosciences Beijing, 29 Xueyuan Road, Beijing 100083, PR China

ARTICLE INFO

Article history:
Received 27 December 2020
Revised 20 February 2021
Accepted 1 April 2021
Available online 20 April 2021

Keywords:
North China Craton
Crustal growth
Zircon U-Pb-Hf isotopes
Neoarchean-Paleoproterozoic
Changcheng Group

ABSTRACT

Late Neoarchean-Paleoproterozoic marks a major period of continental growth and recycling, the culmination of which witnessed the assembly of the Columbia supercontinent and its subsequent breakup. The North China Craton (NCC) preserves important records of tectonic activities and crust building and recycling processes during this time. In this study, we carried out U-Pb geochronology and Lu-Hf isotopic analyses of detrital zircon grains from four sedimentary formations of the Changcheng Group in the Yanliao intracontinental rift in NE NCC. Our isotopic ages constrain the timing of initiation of the Yanliao rift as ca. 1680 Ma. The zircon U-Pb data show two major age populations at 2.7–2.5 Ga and 2.2–1.9 Ga, with high and positive $\varepsilon_{Hf}(t)$ values of + 0.1 to + 34.6. Both the Neoarchean and Paleoproterozoic detrital zircon populations were derived from the basement rocks of the NCC. The results from our study indicate major juvenile crust accretion during Neoarchean and Paleoproterozoic associated with the craton building process of the NCC.

1. Introduction

The mechanism, timing and volumes of continental crustal growth during the early history of Earth have been of wide interest and research on these frontier themes have provided important insights into the evolution of continents through time (e.g., Cawood and Hawkesworth, 2019; Hawkesworth et al., 2019; Palin and Santosh, 2020). Crustal growth at convergent margins is accomplished by tectonic accretion of intra-oceanic island arcs or magmatic additions at continental arcs (Furnes et al., 2020; Santosh, 2013; Tian and Xiao, 2020). Precambrian terranes provide windows to the processes of continental growth and recycling, cratonization and intra-cratonic processes (e.g., Jayananda et al., 2020; Santosh et al., 2020a). Granitoids as the major components of continental crust commonly display enriched Sm-Nd and Lu-Hf isotope composition and were interpreted as a result of recycling of older crust (Allegre and Othman, 1980; Darbyshire and Shepherd, 1994; Liew and Hofmann, 1988). This has led to the concept that the present-day continent crust is what is preserved from its growth during the Precambrian era with only little addition during the Phanerozoic. However, recent studies have shown that substantial volumes of new crustal growth have occurred in the younger Earth, such as in the case of the Central Asian Orogenic Belt, the largest Phanerozoic orogen in the world (Geng et al., 2009; Tang et al., 2012a, 2012b, 2012c).

The North China Craton (NCC), one of the oldest cratons in the world has been in focus for investigations related to episodic crustal growth during Neoarchean and Paleoproterozoic (Fig. 1; Shi et al., 2019, 2012; Tang and Santosh, 2018a; Zhai and Santosh, 2011; Zhou et al., 2014). Previous studies suggested that the oldest crust of the NCC might have formed at 4.0–3.8 Ga, and ca. 3.8–3.7 Ga detrital zircon grains were found in the Proterozoic and Paleozoic strata in central, southern and northeastern sections of the NCC, indicating an Eoarchean crust growth event (Tang and Santosh, 2018a; Zhai and Santosh, 2011, 2013). Zhai and Santosh (2011) reviewed the Precambrian magmatic events in the NCC, and proposed that 78% of these occurred during 3.0–2.5 Ga, 15% during pre-3.0 Ga, and 7% during post-2.5 Ga. The 3.0–2.5 Ga magmatic phases have been subdivided into two pluses at 2.9–2.7 Ga and 2.6–2.5 Ga. The former is coeval with the world-wide 2.8–2.7 Ga Tonalite-Trondhjemite-Granodiorite (TTG) suite of rocks,

* Corresponding author.
E-mail address: liuhuichuan1986@126.com (H. Liu).

https://doi.org/10.1016/j.gr.2021.04.001
1751-7311/

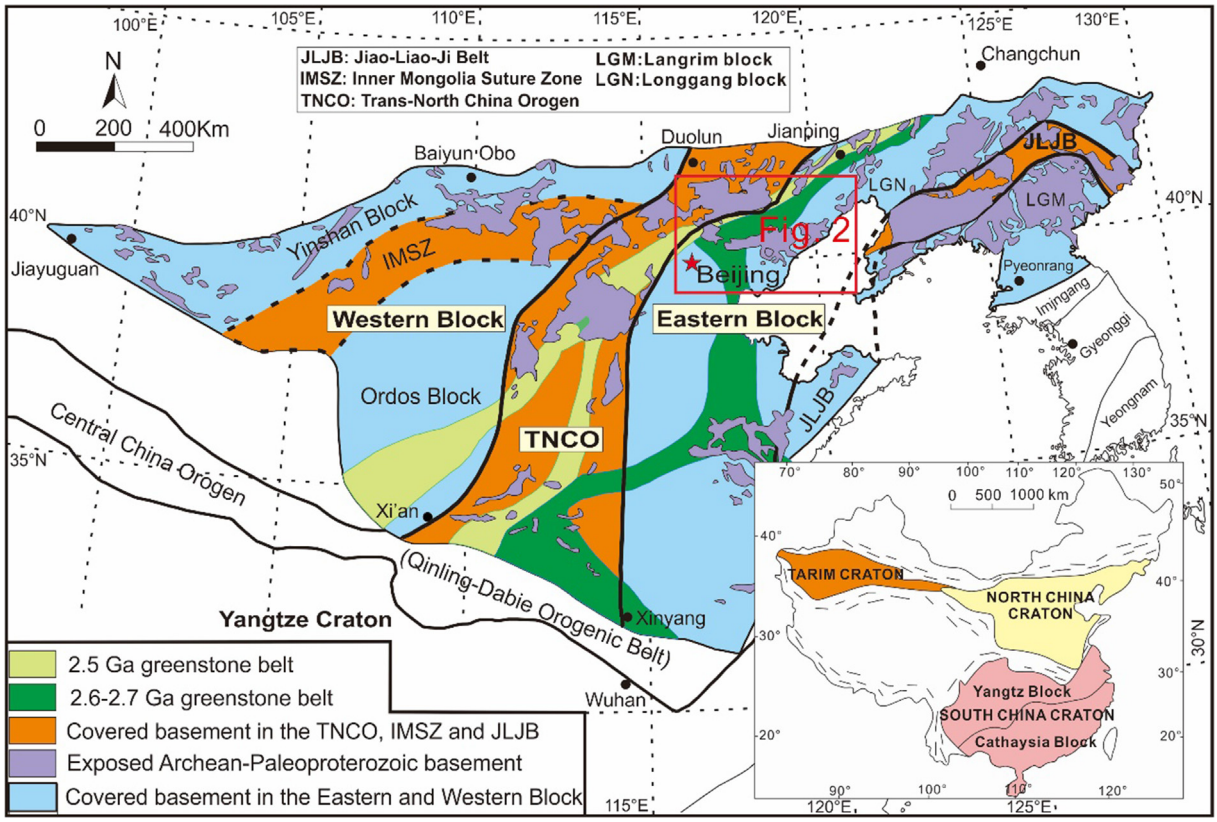

Fig. 1. (a) General geological and tectonic framework of the crustal blocks and orogenic belts in the North China Craton (after Santosh et al., 2020b).

marking the most significant crust growth event in earth history. Late Neoarchean-Paleoproterozoic was a key period for the construction of Earth's first coherent supercontinent, the Columbia supercontinent during Paleoproterozoic, and its subsequent breakup (Meert, 2012; Meert and Santosh, 2017; Palin et al., 2020). As an important crustal fragment within the Columbia assembly, the Precambrian crustal evolution history of the NCC is of wide interest. In the NE NCC, the Yanliao rift basin developed thick Paleoproterozoic to Neoproterozoic (1.8 to 0.80 Ga) sedimentary strata (Figs. 1-3), and provided us an ideal area for investigating the Precambrian crustal evolution history of the NCC.

Zircon is a common accessory mineral in crustal lithologies, and is resistant to hydrothermal alteration, weathering and other secondary processes (Hawkesworth and Kemp, 2006; Kemp et al., 2010). Zircon Lu-Hf isotopes provide important information on the nature of primary magmas (Hawkesworth and Kemp, 2006; Kemp et al., 2009). Thus, combined zircon U-Pb ages and Lu-Hf isotope compositions are powerful tracers to reveal crustal growth and recycling events (Griffin et al., 2004; Hawkesworth and Kemp, 2006; Santosh et al., 2020a). In this contribution, we present zircon U-Pb ages and Lu-Hf isotopes on a suite of sedimentary strata from four formations of the Changcheng Group within the Yanliao rift zone in the North China Craton (Figs. 1, 2 and 3). Based on the results, we evaluate the depositional ages and provenance of these sediments and discuss their implications on the Neoarchean-Paleoproterozoic crust growth events of the NCC.

2. Geological background and sampling

The North China Craton, covering an area of 1.3×10^6 km^2, is bounded by the Qilian Orogen to the west, the Central Asian Orogenic Belt to the north, the Qinling-Dabie Orogenic Belt to the south and the Sulu ultrahigh-pressure metamorphic belt to the east, respectively (Fig. 1; Zhao et al., 2005; Santosh, 2010). The NCC was formed by the amalgamation of two major continental blocks, the Eastern Block (EB) and the Western Block (WB), along the Trans-North China Orogen (TNCO) and the final collision of these blocks is considered to have occurred during the Late Paleoproterozoic at ca. 1.85 Ga (Zhai and Santosh, 2011; Zhao et al., 2005). The WB is composed by the Yinshan and Ordos blocks that were amalgamated along the Khondalite Belt at ~1.95 Ga (Zhao and Zhai, 2013). The EB can be divided into the Longgang and Langrim blocks separated by the Paleoproterozoic Jiao-Liao-Ji Belt (Fig. 1; Zhao et al., 2012; Zhao and Zhai, 2013). The TNCO is dominated by Paleoproterozoic lithotectonic assemblages but also contains abundant Neoarchean supracrustal rocks, TTGs and granitoids with sporadic calc-alkaline volcanics and clastic sediments (Zhao et al., 2005; 2012;; Tang and Santosh, 2018a; Gao and Santosh, 2020).

The Eastern Block preserves Archean basement which includes both high-grade terranes and low-grade granite–greenstone belts such as those in Southern Jilin, North Liaoning, Anshan-Benxi, Southern Liaoning, Western Liaoning, Eastern Hebei, Miyun, Western Shandong and Eastern Shandong, (Tang and Santosh, 2018a; Wu et al., 2016; Zhao et al., 2012). The TTG gneisses constitute 70% of the total exposure of the Neoarchean basement (Peng et al., 2012a; 2012b;; Santosh, 2010; Wu et al., 2013), and the supracrustal rocks comprise mainly sedimentary and bimodal volcanic rocks (Liu et al., 2014; Wu et al., 2016). All these rocks were deformed and metamorphosed under greenschist- and granulite-facies at ca. 2.48–2.50 Ga (Kusky and Li, 2003; Wu et al., 2013; Zhao et al., 2012; Zhao and Zhai, 2013). The pre-Neoarchean rocks were found only in the Anshan and Eastern Hebei areas (Fig. 2), including fuchsite-bearing quartzites with 3.5–3.85 Ga detrital zircons, the ~3.5 Ga amphibolites in the Caozhuang area of Eastern Hebei, and the 3.3–3.8 Ga granitoids and metasedimentary rocks in the Anshan area (Tang and Santosh, 2018a; Zhai and Santosh,

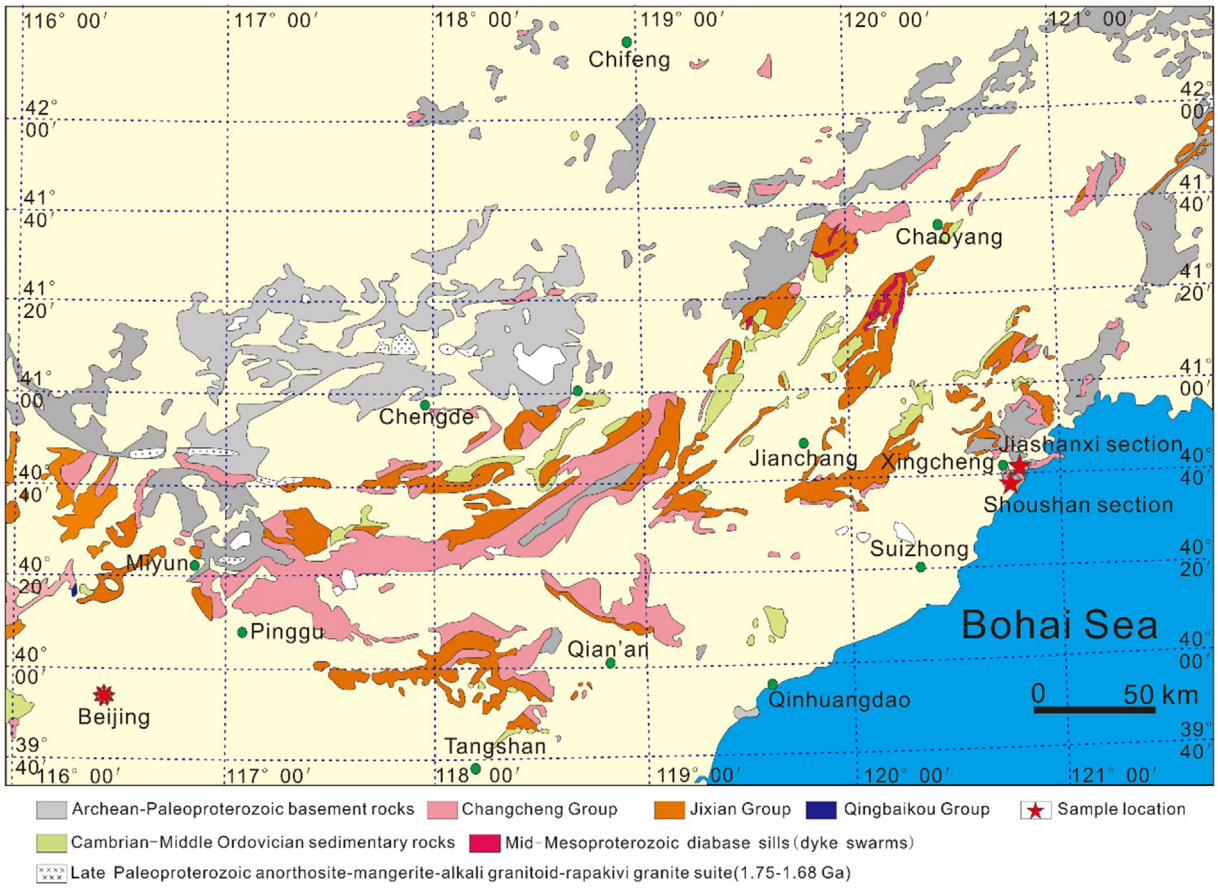

Fig. 2. Simplified geological map of the middle segment of the northern margin of the North China Craton (Wang et al., 2015).

2011). These pre-Neoarchean rocks may have experienced multiple episodes of metamorphism and deformation between 3.8 and 2.5 Ga, but much of their petrographic and isotopic information on the early tectono-thermal events was obliterated by the last metamorphic event at ~2.5 Ga (Shi et al., 2012; Tang and Santosh, 2018b; Zhong et al., 2018). The Paleoproterozoic Jiao-Liao-Ji Belt in the eastern part of the Eastern Block (Fig. 1) is composed of Paleoproterozoic sedimentary and volcanic successions including the Fengzishan and Jingshan Groups in eastern Shandong, the South and North Liaohe Groups in eastern Liaoning, and the Ji'an and Laoling Groups in southern Jilin, which are associated with voluminous Paleoproterozoic granitoid and mafic intrusions (Zhao et al., 2005). Most of the sedimentary and volcanic successions and pre-tectonic (gneissic) granites in the Jiao-Liao-Ji Belt were formed in the period ca. 2200–2000 Ma, and were metamorphosed and deformed at ~1900 Ma (Chen et al., 2013; Zhou et al., 2017).

In the NE NCC, within a major intracontinental rift basin, named the Yanliao rift basin or aulacogen (Fig. 2), deposition of thick sedimentary strata occurred during 1.8 to 0.80 Ga (Wang et al., 2015). The sequence has been divided into four groups and 12 formations with a total thickness of ~9000 m. However, only the lowermost group formed in a rift graben, which extends from east to west and is bounded by deep faults on both sides. The lowermost group is called the Changcheng Group. With a total thickness of around 2700 m, this Group is composed of the Changzhougou, Chuanlinggou, Tuanshanzi and Dahongyu Formations (Fig. 3). The lowermost Changzhougou Formation, unconformably overlying early Precambrian granitic gneiss (Fig. 3), is composed predominantly of conglomerate, pebble-bearing sandstone and arkosic sandstone of fluvial facies in the lower portion and sandstone of marine facies in the middle-upper parts (Fig. 3). Conformably overlying the Changzhougou Formation is the Chuanlinggou Formation that is composed mostly of shales and siltstone (Fig. 3), and is in turn conformably overlain by the dolomite-dominated Tuanshanzi Formation (Fig. 3). The uppermost Dahongyu Formation conformably overlies the Tuanshanzi Formation and consists of littoral and neritic sandstone, shale and potassium-rich trachyte with cherty dolostone in the upper part.

Fifteen samples were collected from the Shoushan and Jiashanxi sections in the Xingcheng area (NE China) for zircon U-Pb geochronology and Lu-Hf isotopic analyses. A summary of the sample details is given in Table 1. The field photographs, as well as the hand-specimen and thin section photomicrographs are shown in Figs. 3 and 4.

The Changzhougou Formation can be divided into three successions. The lower succession is composed of coarse-grained arkoses with cross-bedding forming in an estuary environment. The middle succession consists of thinly-bedded quartz siltstone intercalated with pelitic siltstone and silty mudstone, and the upper succession comprises white, pure sandstone named the "Great Wall Quartz Sandstone". We collected medium-grained sandstone, sandy mudstone and feldspathic sandstone from the Changzhougou Formation. These rocks show high mineral and textural maturity. The Chuanlinggou Formation is composed of three successions, in ascending order, namely black shale with dolomite lenses, thickly-bedded dolomite, and an intercalation of siltstone and thinly-bedded sandstone. We collected one siltstone sample from the middle section of the Chuanlinggou Formation. The Tuanshanzi Formation predominantly consists of muddy and silty dolostone in the lower part and clastic dolomitic sandstone, thin-bedded sandstone and small stromatolitic bioherms in the upper part. Siltstone,

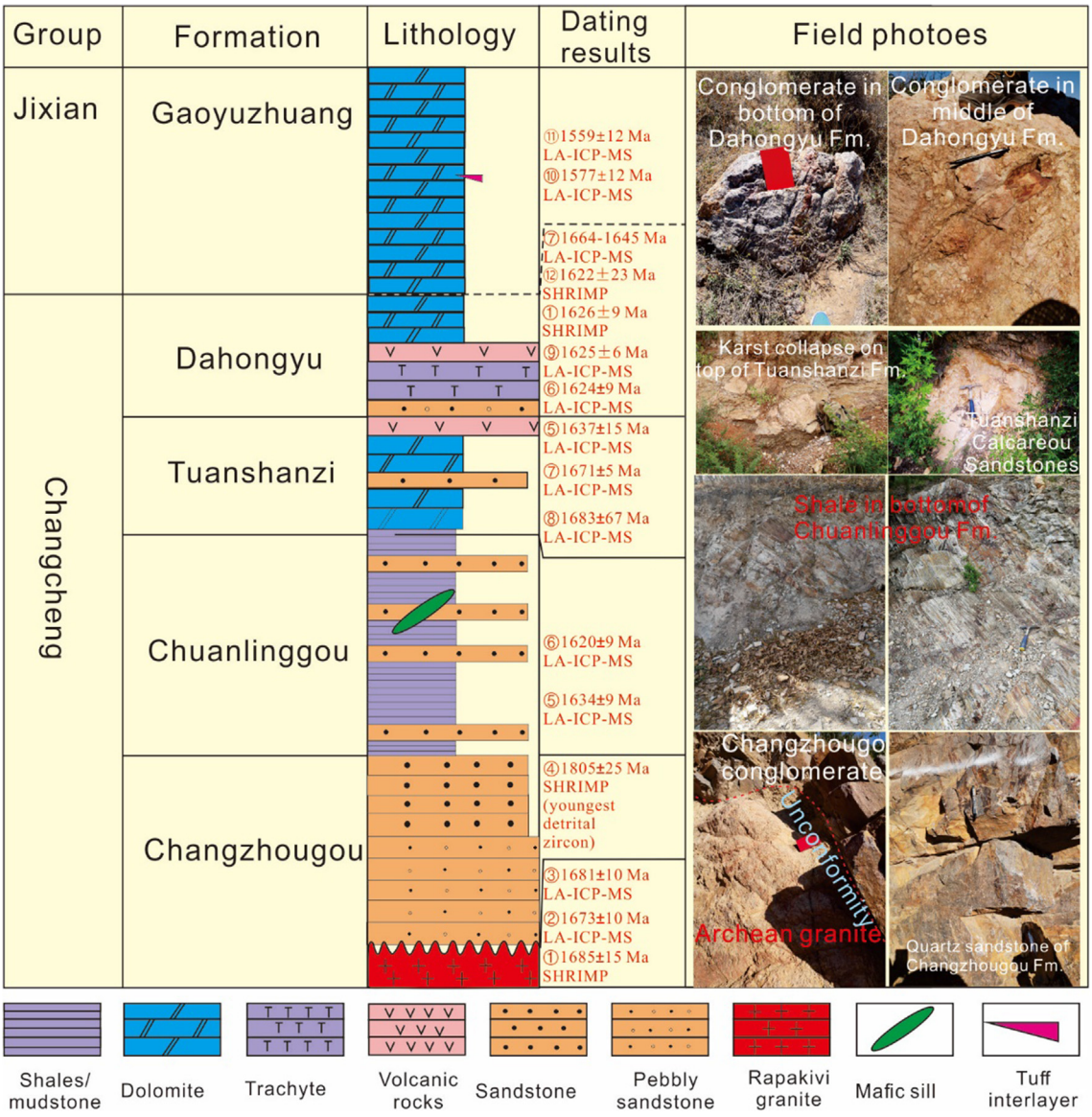

Fig. 3. Stratigraphic column and geochronological framework of the Changcheng Group (after Liu et al., 2019), and photographs of field outcrops. Numbers before the ages refer to the following reference sources: ①-Gao et al., 2008; ②-Li et al., 2011; ③-Yang et al., 2005; ④-Wan et al., 2011; ⑤-Zhang et al., 2013; ⑥-Zhang et al., 2015; ⑦-Wang et al., 2015; ⑧-Li et al., 2013; ⑨-Lu and Li, 1991; ⑩-Tian et al., 2015; ⑪-Li et al., 2010; ⑫-Lu et al., 2008.

sandstone and feldspathic sandstone samples have been selected from the Tuanshanzi Formation. The Dahongyu Formation can also be divided into three successions in ascending order: black shale, silicified rock with Cynobacteria-Oscillatoriopsis fossils, and sandstone beds. Four sandstone samples were selected from Dahongyu Formation.

3. Analytical methods

Zircon U-Pb dating was conducted by LA-ICP-MS at the Wuhan SampleSolution Analytical Technology Co., Ltd., Wuhan, China. Detailed operating conditions for the laser ablation system and the ICP-MS instrument and data reduction are the same as described by Zong et al. (2017). Laser sampling was performed using a GeolasPro laser ablation system that consists of a COMPex-Pro 102 ArF excimer laser (wavelength of 193 nm and maximum energy of 200 mJ) and a MicroLas optical system. An Agilent 7700e ICP-MS instrument was used to acquire ion-signal intensities. Helium was applied as a carrier gas. Argon was used as the make-up gas and mixed with the carrier gas via a T-connector before entering the ICP. A "wire" signal smoothing device is included in this laser ablation system (Hu et al., 2015). The spot size of the laser was set to 30 μm in this study. Zircon 91500 and glass NIST610 were used as external standards for U-Pb dating and trace element calibration, respectively. Each analysis incorporated a background acquisition of approximately 20–30 s followed by 50 s of data acquisition from the sample. An Excel-based software ICPMSDataCal was used to perform off-line selection and integration of background and analyzed signals, time-drift correction and quantitative calibration for trace element analysis and U-Pb dating (Liu et al., 2008, 2010). Concordia diagrams and weighted mean calculations were made using Isoplot/Ex_ver3 (Ludwig, 2003).

The *in-situ* Lu-Hf analysis was conducted using a Neptune Plus MC-ICP-MS (Thermo Fisher Scientific, Germany) in combination with a Geolas HD excimer ArF laser ablation system (Coherent, Göttingen, Germany) that was hosted at the Wuhan Sample

Table 1
Summary of locations, lithology and formations of the representative samples from the Changcheng Group in the Xingcheng area.

Sample No.	Locations	Formations	Rock types
SS-1	Shoushan	Dahongyu (Ch*d*)	Sandstone
SS-3	Shoushan	Tuanshanzi (Ch*t*)	Feldspathic sandstone
SS-6	Shoushan	Chuanlinggou (Ch*ch*)	Siltstone
SS-7	Shoushan	Changzhougou (Ch*c*)	Feldspathic sandstone
SS-8	Shoushan	Changzhougou (Ch*c*)	Sandy mudstone
SS-9	Shoushan	Changzhougou (Ch*c*)	Sandy mudstone
JSX-1	Jiashanxi	Dahongyu (Ch*d*)	Sandstone
JSX-2	Jiashanxi	Dahongyu (Ch*d*)	Sandstone
JSX-3	Jiashanxi	Dahongyu (Ch*d*)	Sandstone
JSX-3-2	Jiashanxi	Dahongyu (Ch*d*)	Sandstone
JSX-4	Jiashanxi	Tuanshanzi (Ch*t*)	Sandstone
JSX-5	Jiashanxi	Tuanshanzi (Ch*t*)	Siltstone
JSX-6	Jiashanxi	Tuanshanzi (Ch*t*)	Pelitic siltstone
JSX-9	Jiashanxi	Changzhougou (Ch*c*)	Medium-grained sandstone
JSX-10	Jiashanxi	Changzhougou (Ch*c*)	Medium-grained sandstone

Solution Analytical Technology Co., Ltd, Hubei, China. A "wire" signal smoothing device is included in this laser ablation system, by which smooth signals are produced even at very low laser repetition rates down to 1 Hz (Hu et al., 2015). Helium was used as the carrier gas within the ablation cell and was merged with argon (makeup gas) after the ablation cell. Small amounts of nitrogen were added to the argon makeup gas flow for the improvement of sensitivity of Hf isotopes (Hu et al., 2012). Compared to the standard arrangement, the addition of nitrogen in combination with the use of the newly designed X skimmer cone and Jet sample cone in Neptune Plus improved the signal intensity of Hf, Yb and Lu by a factor of 5.3, 4.0 and 2.4, respectively. All data were acquired on zircon in single spot ablation mode at a spot size of 44 μm. The energy density of laser ablation that was used in this study was ~ 7.0 J cm^{-2}. Each measurement consisted of 20 s of acquisition of the background signal followed by 50 s of ablation signal acquisition. Detailed operating conditions for the laser ablation system and the MC-ICP-MS instrument and analytical method are the same as the description by Hu et al. (2012).

4. Results

4.1. 1. Geochronological data

4.1.1. Changzhougou Formation

Zircon grains from 15 samples were analyzed for U-Pb. Optical and cathodoluminescence (CL) imaging reflects typical source-proximal (e.g., angular grains) and igneous origin (oscillatory zoning) features (Figs. 5–7).

Fifty analyses on sample JSX-10 yielded mostly high Th/U ratios (0.3 – 2.5; Supplementary Table S1). Forty-two of the spots fall along a lead-loss line with the upper intercept at 2602 ± 55 Ma (Fig. 5a). These analyses yielded $^{207}Pb/^{206}Pb$ ages ranging between 2.11 Ga and 2.68 Ga, with one major age peak at 2.55 Ga and a minor peak at 2.15 Ga.

Sample JSX-9 is sandstone from the middle section of the Changzhougou Formation (Chc). The zircons are commonly 60–150 μm in size, round and ellipsoidal in shape, and show oscillatory zoning in CL image (Fig. 5b). A total of fifty analyses were made on 50 zircons. Their Th/U ratios range from 0.2 to 1.9 (Supplementary Table S1). Forty-six analyses show lead loss and fall along a lead-loss line with the upper intercept at 2583 ± 18 Ma (Fig. 5b). Their $^{207}Pb/^{206}Pb$ ages range from 2.20 Ga to 2.69 Ga, and show a significant age peak at 2.60 Ga.

Fifty analyses were performed on sample SS-9, and their Th/U ratios range from 0.4 to 2.3. Most analyses are discordant and fall along a Pb loss line with the upper intercept at 2581 ± 22 Ma (Fig. 5c). These analyses show a wide range of $^{207}Pb/^{206}Pb$ ages between 2.49 Ga and 2.78 Ga.

Forty-eight analyses were performed on sample SS-8. The zircons are medium grained (mostly 60–100 μm), round or stubby in shape, and show oscillatory zoning or homogeneous structures in CL images (Fig. 5d). Eleven analyses were excluded due to erroneous $^{207}Pb/^{206}Pb$ ages. The remaining 37 analyses show lead loss

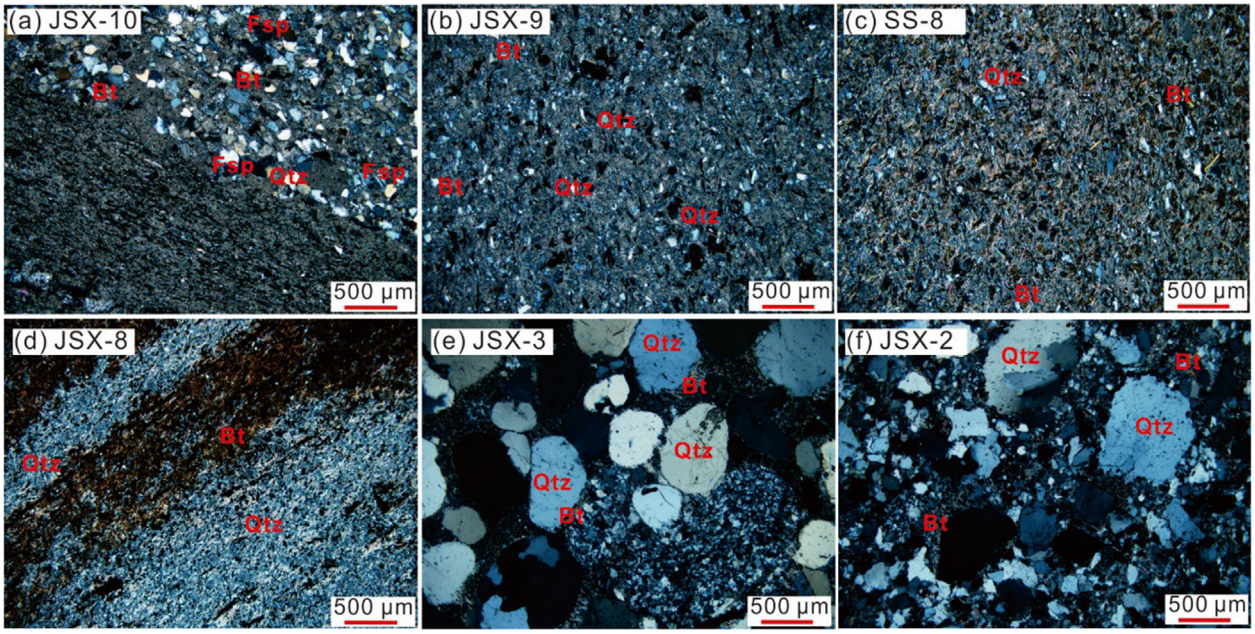

Fig. 4. Photomicrographs of the Changzhougou Formation. Mineral abbreviations: Bt-Biotite; Qtz-Quartz; Fsp-Feldspar.

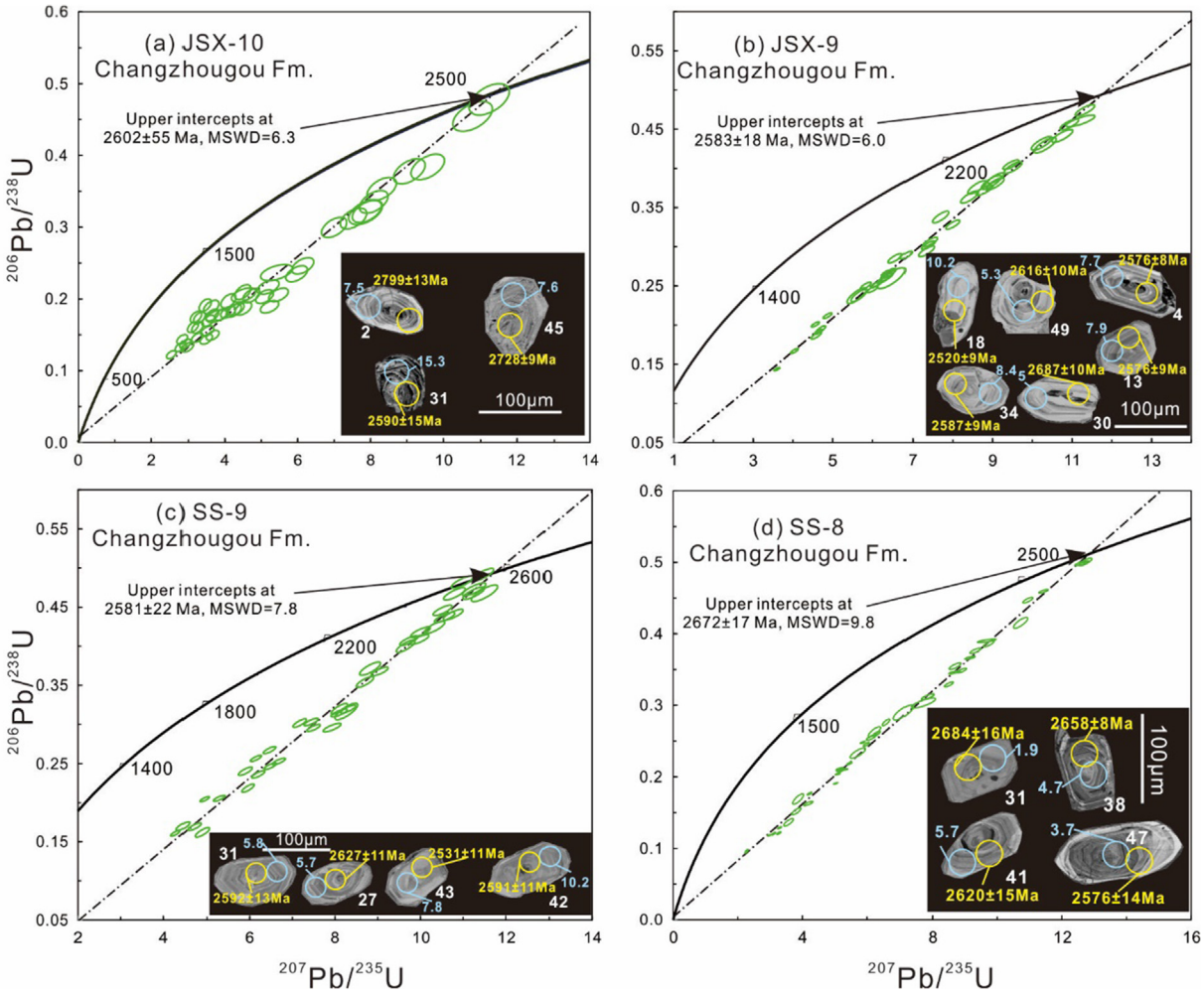

Fig. 5. Zircon U-Pb Concordia diagrams and representative zircon Cathodoluminescence (CL) images of the Changzhougou Formation. The yellow circles indicate the U-Pb isotopic spots, and the wathet circles represent the domains of Lu-Hf isotopic analyses. (For interpretation of the references to colour in this figure legend, the reader is referred to the web version of this article.)

and fall along a lead-loss line with the upper intercept at 2678 ± 22 Ma (Fig. 5d). Their $^{207}Pb/^{206}Pb$ ages show a range of 2.52 Ga and 2.72 Ga with a significant peak at 2.6 Ga.

Sample SS-7 was taken from the upper section of the Changzhougou Formation (Chc), and 50 analyses were performed on this sample. The zircons mostly medium grained (mostly 70–150 μm), stubby in shape, and show oscillatory zoning in CL images (Fig. 6a). Fifteen of these were excluded due to high error. The remaining 35 analyses show lead loss (Fig. 6a) and fall along a lead-loss line with the upper intercept at 2597 ± 36 Ma. Their $^{207}Pb/^{206}Pb$ ages show a range of 2.41 Ga and 2.69 Ga with a significant peak at 2.6 Ga.

4.1.2. Chuanlinggou Formation

We collected four mudstone and siltstone samples from the Chuanlinggou Formation, but only one sample contains enough zircons for U-Pb dating. We carried out 33 U-Pb analyses on zircon grains from sample SS-6, and they show high and variable Th/U ratios of 0.3 – 2.2. Eleven of these were excluded due to high error. The remaining analyses are discordant (Supplementary Fig. S1a), yielding an age peak at 2.55 Ga.

4.1.3. Tuanshanzi Formation

Fifty analyses on sample JSX-6 yielded mostly high Th/U ratios (0.3 – 2.7), (Supplementary Table S1), consistent with an igneous origin. Most analyses are discordant, and Forty of them fall along a lead-loss line with the upper intercept at 2587 ± 40 Ma (Fig. 6b). These analyses yielded $^{207}Pb/^{206}Pb$ ages ranging between 2.09 and 2.68 Ga, with one major age peak at 2.55 Ga.

Fifty analyses were performed on sample JSX-4, and their Th/U ratios range from 0.3 to 4.4. Twelve analyses were excluded due to erroneous $^{207}Pb/^{206}Pb$ ages. Most analyses are discordant due to significant lead loss, and fall along a line with the upper intercept at 2525 ± 18 Ma (Fig. 6c). These analyses show a wide range of $^{207}Pb/^{206}Pb$ ages between 2.48 Ga and 2.91 Ga with one major peak at 2.58 Ga.

Forty analyses were performed on sample SS-3. The zircons are medium sized (mostly 60–100 μm), round or stubby in shape, and show oscillatory zoning or homogeneous structures in CL images (Fig. 6d). Eight analyses were excluded due to erroneous $^{207}Pb/^{206}Pb$ ages. The remaining 37 analyses show lead loss (Fig. 6d) and fall along a lead-loss line with the upper intercept at 2597 ± 26 Ma. Their $^{207}Pb/^{206}Pb$ ages show a range of 1.92 Ga and 2.72 Ga with a significant peak at 2.60 Ga.

Sample JSX-5 is siltstone from the middle section of the Tuanshanzi Formation (Cht). The zircons are commonly 60–150 μm in size, ellipsoidal in shape, and show oscillatory zoning in CL image (Supplementary Fig. S2b). A total of forty-six analyses were made on 46 zircons. Their Th/U ratios range from 0.1 to 3.1 (Supplementary Table S1). Twenty-two analyses show lead loss and fall along

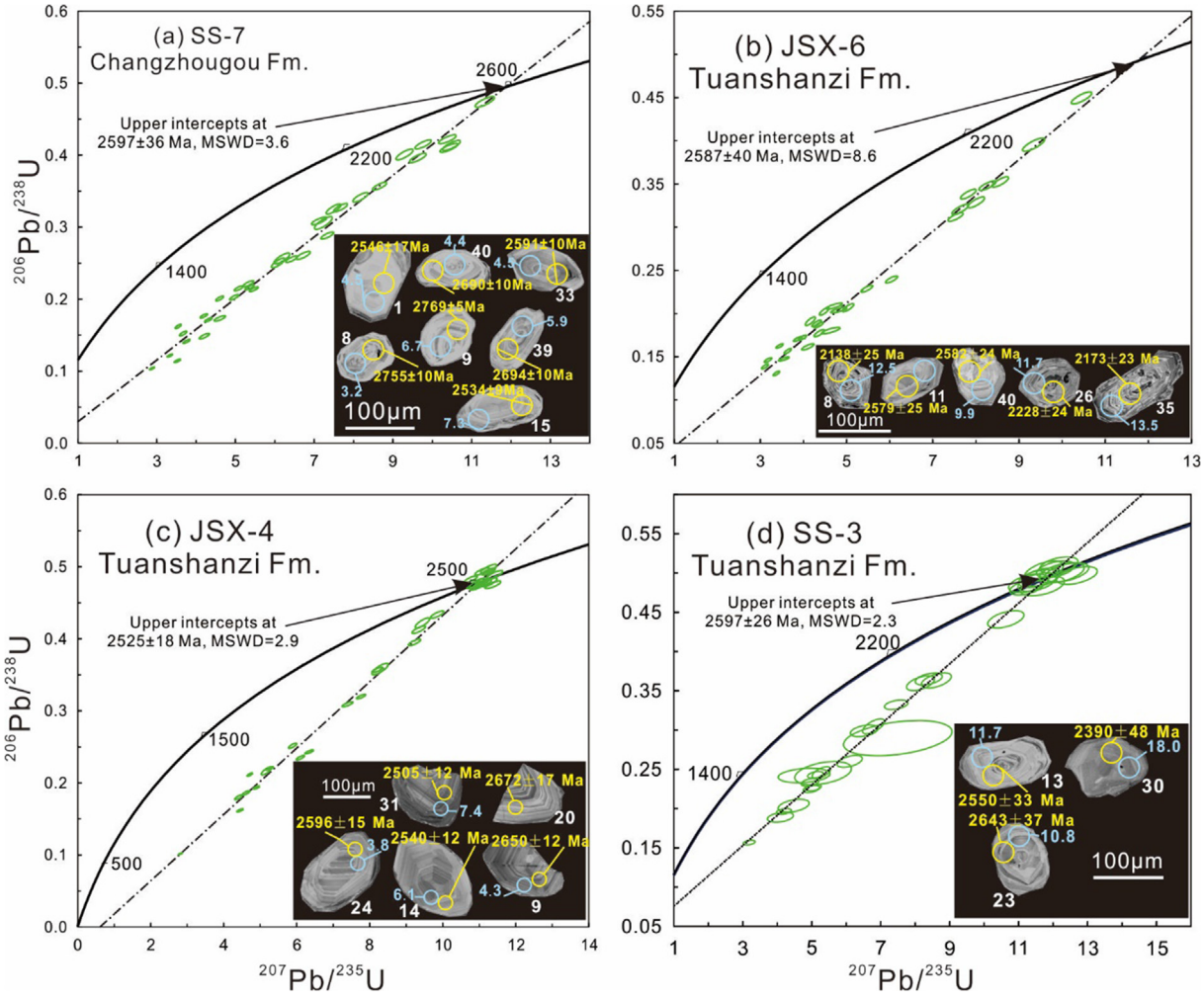

Fig. 6. Zircon U-Pb Concordia diagrams and representative zircon Cathodoluminescence (CL) images of the Changzhougou (a and b) and Tuanshanzi (c and d) formations. The yellow circles indicate the U-Pb isotopic spots, and the white circles represent the domains of Lu-Hf isotopic analyses. (For interpretation of the references to colour in this figure legend, the reader is referred to the web version of this article.)

two lead-loss lines with the upper intercept at 1920 ± 54 Ma and 2734 ± 35 Ma (Supplementary Fig. S2b).

4.1.4. Dahongyu Formation

Forty analyses were performed on sample JSX-3, and their Th/U ratios range from 0.5 to 2.0. The forty analyses could be subdivided into two groups, and most analyses are discordant due to significant lead-loss. These analyses fall along two lead-loss lines with the upper intercepts at 2118 ± 48 Ma and 2508 ± 21 Ma (Fig. 7a). These analyses show a wide range of $^{207}Pb/^{206}Pb$ ages between 2.48 Ga and 2.91 Ga with one major peak at 2.58 Ga. The younger group shows $^{207}Pb/^{206}Pb$ ages of 1.98 Ga and 2.23 Ga, and the older group shows $^{207}Pb/^{206}Pb$ ages of 2.33 Ga and 2.58 Ga.

Sample JSX-3–2 was taken from the lower section of the Dahongyu Formation (Ch*d*), and 25 analyses were performed on zircons from this sample. The zircons are medium in size (mostly 70–140 μm), stubby in shape, and show oscillatory zoning in CL images. Ten analyses were excluded due to their erroneous $^{207}Pb/^{206}Pb$ ages. The remaining 15 analyses show severe lead loss (Supplementary Fig. S2c) and fall along a lead-loss line with the upper intercept at 2631 ± 77 Ma. Their $^{207}Pb/^{206}Pb$ ages show a range of 2.11 Ga and 2.80 Ga with a significant peak at 2.65 Ga.

Sample JSX-2 is sandstone from the middle section of the Dahongyu Formation (Ch*d*). The zircons are commonly 100–150 μm in size, round and ellipsoidal in shape, and show oscillatory zoning in CL image (Fig. 7b). A total of fifty analyses were made on 50 zircons. Their Th/U ratios range from 0.1 to 1.2 (Supplementary Table S1). Thirteen analyses were excluded due to erroneous $^{207}Pb/^{206}Pb$ ages. Most analyses show lead loss and fall along a lead-loss line with the upper intercept at 2078 ± 44 Ma (Fig. 7b). Their $^{207}Pb/^{206}Pb$ ages range from 1.96 Ga to 2.74 Ga, and show two significant age peaks at 2.15 Ga and 2.60 Ga.

Fifty analyses on sample JSX-1 yielded mostly high Th/U ratios (0.1 – 3.6), (Supplementary Table S1). With five analyses excluded due to their discordance and plotting far away from the pervasive Pb loss line, the remaining data fall along a lead-loss line with the upper intercept at 2581 ± 27 Ma (Fig. 7c). These analyses yielded $^{207}Pb/^{206}Pb$ ages ranging between 1.81 Ga and 2.77 Ga, with one age peak at 2.55 Ga.

Fifty analyses were performed on sample SS-2. The zircons are medium in size (mostly 50–120 μm), round or stubby in shape, and show oscillatory zoning or homogeneous structures in CL images. Four analyses are excluded due to high error. The remaining 46 analyses show significant lead loss (Supplementary Fig. S2d). Their $^{207}Pb/^{206}Pb$ ages show a range of 1.96 Ga and 2.68 Ga with two significant peaks at 2.10 Ga and 2.60 Ga.

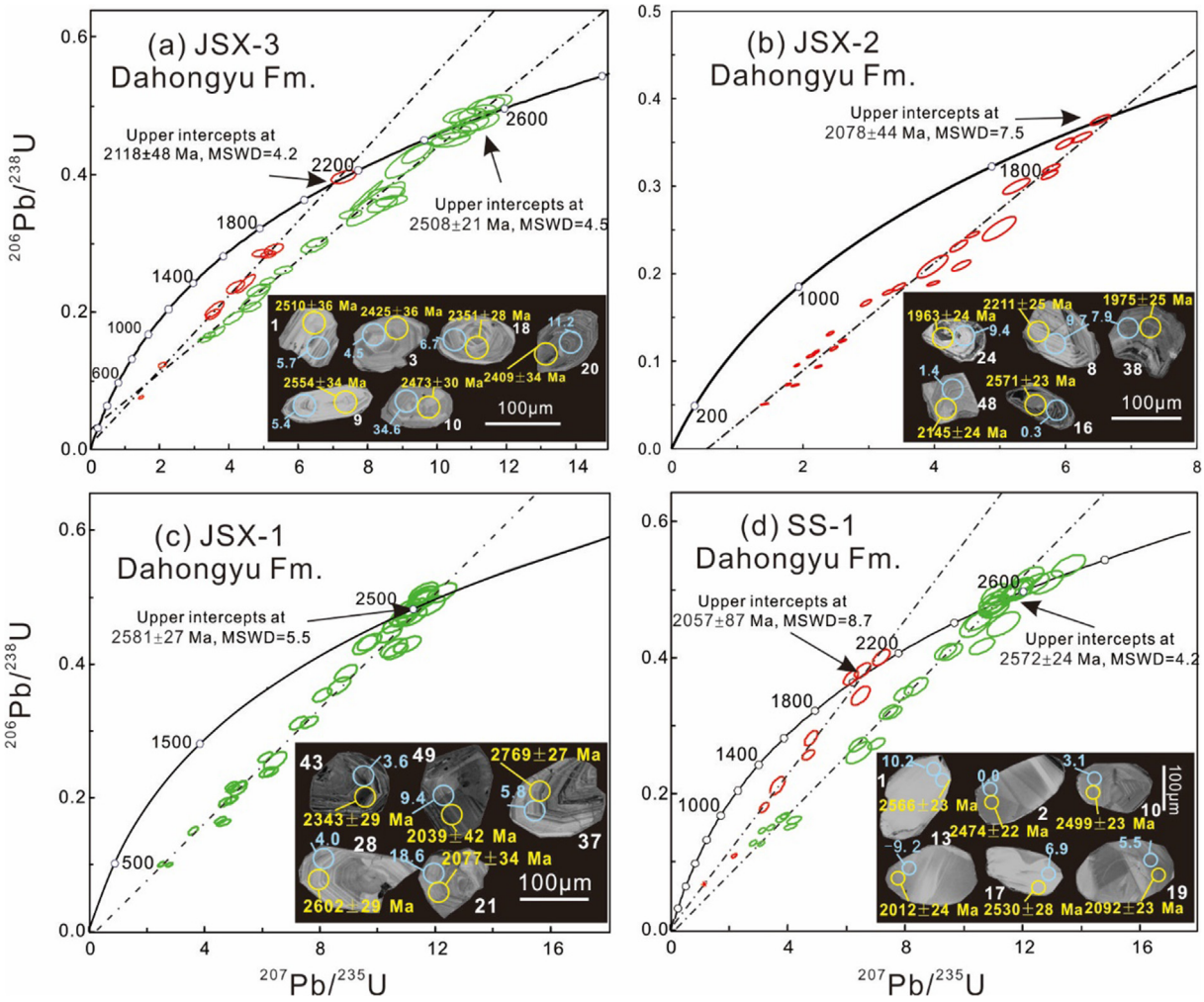

Fig. 7. Zircon U-Pb Concordia diagrams and representative zircon Cathodoluminescence (CL) images of the Dahongyu Formation. The yellow circles indicate the U-Pb isotopic spots, and the wathet circles represent the domains of Lu-Hf isotopic analyses. (For interpretation of the references to colour in this figure legend, the reader is referred to the web version of this article.)

Fifty analyses were performed on sample SS-1, and their Th/U ratios range from 0.3 to 2.6. Twenty-seven analyses are discordant due to significant lead-loss, and fall along two lead-loss lines with the upper intercepts at 2057 ± 87 Ma and 2572 ± 24 Ma (Fig. 7d). These analyses show a wide range of $^{207}Pb/^{206}Pb$ ages between 1.91 Ga and 2.69 Ga with two peaks at 2.15 Ga and 2.55 Ga.

We compiled all the published detrital zircon U-Pb ages about the Changcheng Group in Fig. 8. The Changzhougou and Tuanshanzi formations show one significant peak at 2.60 Ga and 2.65 Ga, respectively. The Chuanlinggou and Dahongyu formations show two age peaks at 2.00 Ga and 2.55 Ga, and 2.10 Ga and 2.60 Ga, respectively.

4.2. Zircon in-situ Lu-Hf isotopes

Zircon Lu-Hf isotopic results for the dated samples are listed in Supplementary Table S2 and shown on Figs. 9 and 10. Initial Hf isotopic ratios are recalculated based on their upper intercept ages, using the ^{176}Lu–^{176}Hf decay constant reported by (Soderlund et al., 2004). $^{176}Lu/^{177}Hf$ ratios of most zircons are less than 0.003 (Supplementary Table S2), indicating a low radiogenic growth of ^{176}Hf. Two-stage model ages (T_{DM2}) are calculated for the source of magma by assuming a mean $^{176}Lu/^{177}Hf$ value of 0.015 for the average continental crust (Griffin et al., 2002).

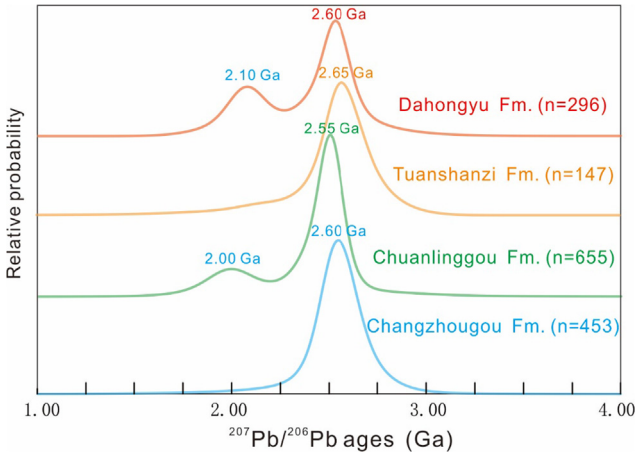

Fig. 8. Relative probability plots of detrital zircon U-Pb ages from the four formations of the Changcheng Group. Data are from our studies and references (Lamb et al., 2009; Lu et al., 2002; Meng et al., 2011; Miao et al., 2019; Wan et al., 2011; Wang et al., 2015).

4.2.1. Changzhougou Formation

Fifteen Lu–Hf analyses were performed on 15 zircons from the sample JSX-10 (Supplementary Table S2). These spots have high

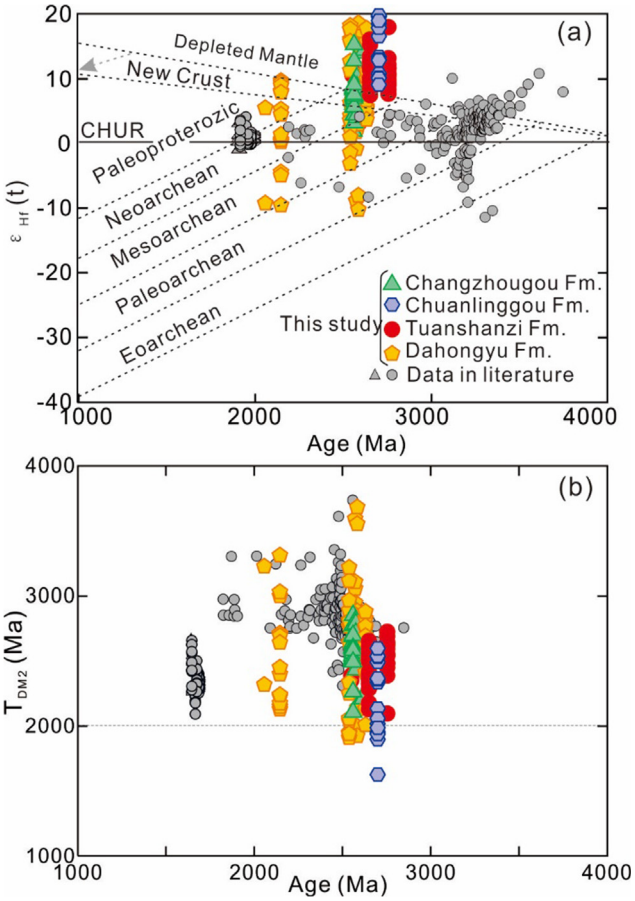

Fig. 9. (a) Zircon U-Pb ages (Ma) vs. $\varepsilon_{Hf}(t)$ values; and (b) U-Pb ages (Ma) vs. T_{DM2} for samples from the Changcheng Group. CHUR-chondritic uniform reservoir. The new crust line is from (Dhuime et al., 2011). Data are from our studies and references (Meng et al., 2011; Wan et al., 2011; Wang et al., 2015). Due to the scarcity of the concordant grains falling on the Concordia, upper intercept ages were used to calculate the initial epsilon Hf values.

and positive $\varepsilon_{Hf}(t)$ values of + 5.7–+15.3 and relatively young two-stage Hf model ages (T_{DM2} = 2.1–2.7 Ga) compared with their zircon U-Pb ages (Figs. 9 and 10; Supplementary Table S2).

Fifteen Lu–Hf analyses were performed on 15 zircons from the sample JSX-9 (Supplementary Table S2). These spots have high and positive $\varepsilon_{Hf}(t)$ values of + 4.1 – +14.4 and relatively young two-stage Hf model ages (T_{DM2} = 2.2–2.8 Ga) compared with their zircon U-Pb ages (Fig. 9; Supplementary Table S2).

Fifteen Lu–Hf analyses were performed on 15 zircons from the sample SS-9 (Supplementary Table S2). These spots also show high and positive $\varepsilon_{Hf}(t)$ values of + 4.0 – +10.2 and relatively young two-stage Hf model ages (T_{DM2} = 2.4–2.8 Ga) compared with their zircon U-Pb ages (Fig. 9; Supplementary Table S2).

Eleven Lu–Hf analyses on 11 zircons from the sample SS-8 (Supplementary Table S2) yielded high and positive $\varepsilon_{Hf}(t)$ values of + 1.9 – +16.6 and relatively young two-stage Hf model ages (T_{DM2} = 2.0–2.9 Ga) compared with their zircon U-Pb ages (Fig. 9; Supplementary Table S2).

Fourteen Lu–Hf analyses on 14 zircons from the sample SS-7 (Supplementary Table S2) show high and positive $\varepsilon_{Hf}(t)$ values of + 3.2 – +8.7 and relatively young two-stage Hf model ages (T_{DM2} = 2.5–2.9 Ga) compared with their zircon U-Pb ages (Fig. 9; Supplementary Table S2).

4.2.2. Chuanlinggou formation

Fifteen Lu–Hf analyses on 15 zircons from the siltstone sample SS-6 (Supplementary Table S2) show high and positive $\varepsilon_{Hf}(t)$ values

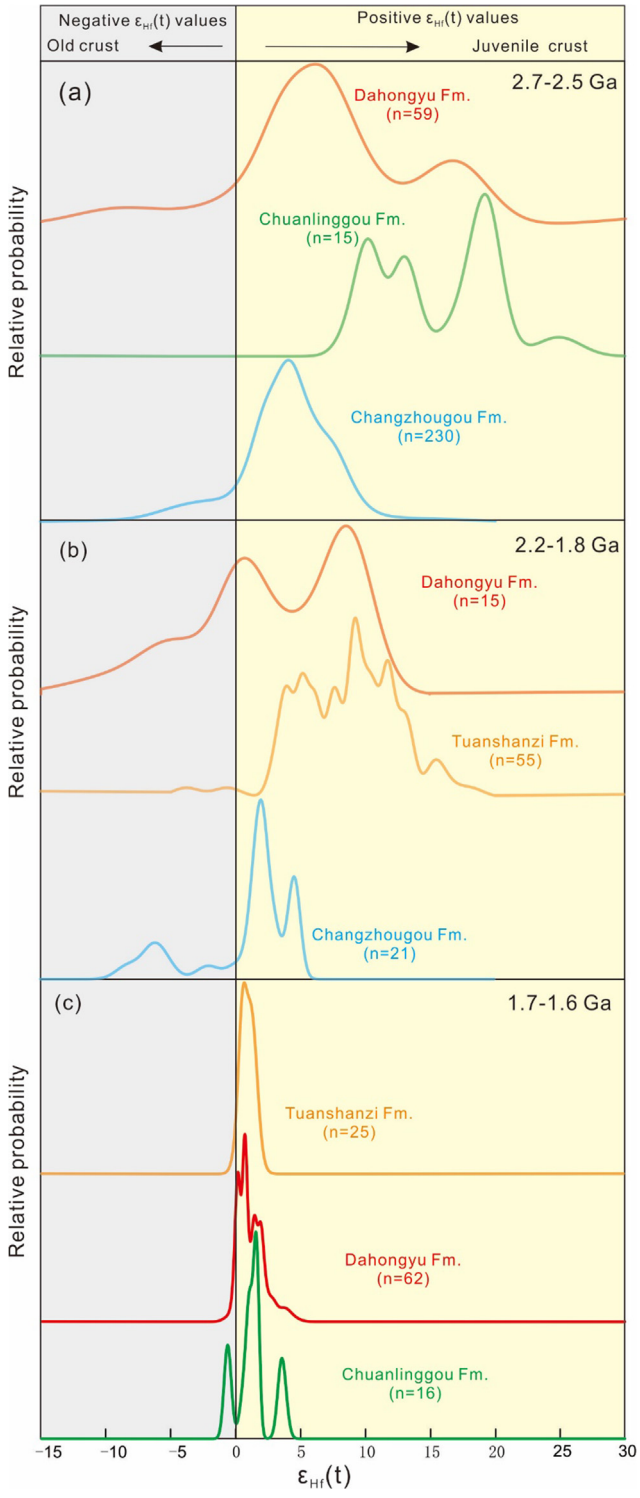

Fig. 10. Probability density plots of the detrital zircon $\varepsilon_{Hf}(t)$ values showing the differences of the two major age populations at 2.7 – 2.5 Ga (a) and 2.2 – 1.9 Ga (b). Probability density plots of the zircon $\varepsilon_{Hf}(t)$ values of the late Paleoproterozoic (1.71 – 1.62 Ga) volcanic and intrusive rocks identified in the Changcheng Group. Data are from our studies and references (Meng et al., 2011; Wan et al., 2011; Wang et al., 2015).

of + 6.8 – +22.9 and relatively young two-stage Hf model ages (T_{DM2} = 1.7–2.7 Ga) (Figs. 9 and 10; Supplementary Table S2).

4.2.3. Tuanshanzi formation

Fourteen Lu–Hf analyses on 14 zircons from the sample JSX-6 (Supplementary Table S2) yield high and positive $\varepsilon_{Hf}(t)$ values

of + 7.5 – +16.1 and relatively young two-stage Hf model ages (T_{DM2} = 2.1–2.7 Ga) compared with their zircon U-Pb ages (Figs. 9 and 10; Supplementary Table S2).

Among the fourteen Lu–Hf analyses on 14 zircons from the sample JSX-5 (Supplementary Table S2), except two spots (JSX-5–20 and JSX-5–36) with negative $\varepsilon_{Hf}(t)$ values (-0.6 and −3.8), the remaining 12 spots show a range of positive $\varepsilon_{Hf}(t)$ values (+3.1 – +35.8), and relatively young two-stage Hf model ages (T_{DM2} = 0.3–2.6 Ga) compared with their zircon U-Pb ages (Fig. 9).

Fourteen Lu–Hf analyses on 14 zircons from the sample SS-3 (Supplementary Table S2) show high and positive $\varepsilon_{Hf}(t)$ values of + 7.7 – +18.0 and relatively young two-stage Hf model ages (T_{DM2} = 2.1–2.7 Ga) compared with their zircon U-Pb ages (Fig. 9; Supplementary Table S2).

4.2.4. Dahongyu formation

Fifteen Lu–Hf analyses on 15 zircons from the sample JSX-3 (Supplementary Table S2) yield high and positive $\varepsilon_{Hf}(t)$ values of + 3.7 – +34.6 and relatively young two-stage Hf model ages (T_{DM2} = 1.0–2.9 Ga) compared with their zircon U-Pb ages (Fig. 9; Supplementary Table S2).

Among the fifteen Lu–Hf analyses on 15 zircons from sample JSX-2, except four spots (JSX-2–39, JSX-2–42, JSX-2–46 and JSX-2–50) with negative $\varepsilon_{Hf}(t)$ values (-29.4, −4.4, −9.5 and −4.9), the remaining 11 zircons have high and positive $\varepsilon_{Hf}(t)$ (+0.3 – +9.7) and relatively young T_{DM2} (2.1–2.7 Ga) (Fig. 9; Supplementary Table S2).

Fifteen Lu–Hf analyses on 15 zircons from sample JSX-1. show two spots (JSX-1–32 and JSX-1–41) with negative $\varepsilon_{Hf}(t)$ value (-1.4 and −3.1), and the remaining13 zircons having high and positive $\varepsilon_{Hf}(t)$ (+3.0 – +34.7) and relatively young T_{DM2} (1.0–2.9 Ga) (Fig. 9; Supplementary Table S2).

Among the fifteen Lu–Hf analyses on 15 zircons from sample SS-2, two spots (SS-2–18 and SS-2–21) show negative $\varepsilon_{Hf}(t)$ value (-1.4 and −3.1), and the remaining 13 zircons have high and positive $\varepsilon_{Hf}(t)$ (+1.0 – +18.2) and relatively young T_{DM2} (1.9–3.0 Ga) (Fig. 9; Supplementary Table S2).

Fourteen Lu–Hf analyses on 14 zircons from sample SS-1 show three spots (SS-1–12, SS-1–26 and SS-1–30) with negative $\varepsilon_{Hf}(t)$ values (-9.2, −0.8 and −8.8), and the remaining with positive $\varepsilon_{Hf}(t)$ (+0.1 – +10.2) and relatively young T_{DM2} (2.3–3.1 Ga) (Fig. 9).

5. Discussion

5.1. Depositional age of the Changcheng Group

The Tuanshanzi and Dahongyu formations of the Changcheng Group contain several layers of voluminous K-rich volcanics (Qu et al., 2014; Wang et al., 2015). Lu et al. (2008) carried out SHRIMP zircon U–Pb dating on trachyte from the upper Dahongyu Formation and obtained a U-Pb age of 1622 ± 23 Ma. A volcanic sample collected from the Dahongyu Formation yielded single-grain zircon U–Pb age of 1625 ± 6 Ma, also interpreted as the age of volcanic eruption (Lu and Li, 1991). Wan et al. (2011) re-analyzed the same volcanic sample from the Dahongyu Formation using the SHRIMP II ion microprobe and obtained an age of 1622 ± 23 Ma, consistent with the conventional single-grain age of 1625 ± 6 Ma. Zhang et al. (2015) carried out SHRIMP zircon U-Pb dating on alkali basalt of the Dahongyu Formation and mafic dyke that intruded into the Chuanlinggou Formation in the Yaoliao rift, and reported ages of 1624 ± 9 Ma and 1620 ± 9 Ma, respectively. Two trachyandesites of the second and third eruption cycles and one sub-alkaline basalt from the fourth eruption cycle of the overlying Dahongyu Formation were dated by Wang et al. (2015) as 1664 ± 6, 1652 ± 7, and 1645 ± 5 Ma, based on the zircon U-Pb method. Thus, the volcanism and sedimentation of the Dahongyu Formation may have lasted from 1664 Ma to 1625 Ma for nearly 40 Myrs.

Zhang et al. (2013) reported a zircon U-Pb age of 1637 ± 15 Ma for potassic volcanic rock from the upper section of the Tuanshanzi Formation at Pinggu in the Beijing city. A single-grain zircon U–Pb upper concordia intercept age of 1683 ± 67 Ma was determined by Li et al. (1995) for a volcanic rock of the Tuanshanzi Formation, interpreted as the age of volcanic eruption. Wang et al. (2015) dated a trachybasalt from the upper section of the Tuanshanzi Formation as 1671 ± 5 Ma, and proposed that the eruption of volcanic rocks and deposition of dolostones with minor shales and sandstones of the Tuanshanzi Formation occurred at ca. 1670 Ma or earlier. Our study clearly establishes the geochronological framework of the stratigraphic sequences in the Changcheng Group (Fig. 3), and we conclude that the Tuanshanzi and Dahongyu Formations formed at ca. 1670 Ma and 1664–1625 Ma, respectively.

One of the key issues is the lowest boundary age of the Changcheng Group, and hence the time of initiation of the Yanliao rift, which was previously considered to be at 1800 Ma, ~1800–1750 Ma, ~1700 Ma, or 1650 Ma, respectively (Lamb et al., 2009; Li et al., 2015; Liu et al., 2019; Lu et al., 2002; Miao et al., 2019; Peng et al., 2009; Wan et al., 2011). No volcanic rocks were found interlayered within the Chuanlinggou and Changzhougou formations, and therefore, their deposition age remained equivocal. Wan et al. (2003) reported detrital SHRIMP U–Pb zircon ages for an arkosic sandstone of the Changzhougou Formation and recognized several zircon populations, among which the youngest is around 1.8 Ga, indicating deposition of the Changzhougou Formation later than 1.8 Ga. Recently, Peng et al. (2012a); (2012b;)) reported ID-TIMS baddeleyite U–Pb age of 1731 ± 4 Ma for a mafic dyke that was unconformably overlain by the sedimentary rocks of the Changzhougou Formation in Miyun, and proposed that the lowest boundary age of the Changcheng Group should be later than 1730 Ma, possibly at ca. 1700 Ma (Fig. 3). Zhang et al. (2015) carried out U-Pb dating on xenotime and monazite grains from the Chuanlinggou Formation and reported the oldest population of 1716 ± 3 Ma, which is interpreted as the minimum depositional age of the Chuanlinggou Formation. Moreover, a vast magmatic belt (~500 km in length) with formation ages of 1680–1750 Ma has been recognized along the northern margin of the NCC. All the 1680–1750 Ma magmatic plutons were emplaced into the Archean basement rocks, and did not intrude the sedimentary cover of the Changcheng Group (i.e. Yanliao rift). All these lines of evidence suggest that the incipient deposition of the Changcheng Group sedimentary rocks probably occurred later than the emplacement of these 1680–1750 Ma magmatic plutons. Accordingly, we propose that the lowest boundary age of the Changcheng Group, corresponding to the initiation of the Yanliao rift, should be earlier than 1671 Ma, but younger than 1680 Ma. Given that there are still two formations (Changzhougou and Chuanlinggou) that lie below the Tuanshanzi Formation (ca. 1671 Ma), the initiation timing of the Yanliao rift can be reasonably constrained as ca. 1680 Ma.

5.2. Provenance of the Changcheng Group

Detrital zircons of the Changcheng Group show two main intervals at 2.7–2.5 Ga and 2.1–1.9 Ga. The ~ 2.7 Ga age data are mainly reported from western and eastern Shandong and some in Zhangjiakou, Guyang, Houqiu and Fuping. Late Neoarchean magmatic rocks are widely distributed in the Eastern Block, Western Block and TNCO with ages varying from 2.55 Ga to 2.48 Ga (Guo et al., 2013; Li et al., 2016; Santosh et al., 2016; 2020b; 2018b;; Shi et al., 2012; Tang and Santosh, 2018a), and they show similar rock associations with TTG rocks, which underwent metamorphism between 2.52 and 2.50 Ga. Similar ~ 2.5 Ga tectonic-magmatic

events are also widely reported from Archean cratons in southern India and Antarctica, and also other coeval cratons (e.g., Jayananda et al., 2020). The sedimentary rocks in our study show poorly-rounded grains that include minor plagioclase feldspar. Thus, the 2.7 – 2.5 Ga detrital zircons are more likely derived from the NCC itself. This conclusion is also evidenced by the zircon Lu-Hf isotopic characteristics. Most of the 2.7 – 2.5 Ga detrital zircons of the Changcheng Group show high and positive $\varepsilon_{Hf}(t)$ values as shown in Fig. 10, which are similar to those of the widely distributed 2.7 – 2.5 Ga magmatic rocks. For example, felsic rocks of the Dengfeng complex (2.75 – 2.48 Ga) show high $\varepsilon_{Hf}(t)$ values of + 5.0 – +9.7 (Shi et al., 2019); granites of the Yishui Complex (2.54 – 2.49 Ga) have $\varepsilon_{Hf}(t)$ values of −2.5 – +5.0 and Neoarchean model ages of 2.92 – 2.70 Ga (Li et al., 2016; Santosh et al., 2017). Diverse Neoarchean granitoid suites from tonalite-trondhjemite-granodiorite (TTG) to potassic granitoids (2.59 – 2.50 Ga) in the Northern Liaoning Province display high $\varepsilon_{Hf}(t)$ values of +0.5 – +8.7 and model ages of 2.84 – 2.54 Ga (Wang et al., 2017).

Regarding the 2.2–1.9 Ga detrital zircons, we interpret that these were also derived from the NCC basement. This conclusion is mainly based on the following observations: (1) Several 2.2 – 2.0 Ga felsic volcanic rocks and plutons are widely exposed in the Daqingshan, northwestern Hebei, Wutai, Lüliang, Zhongtiaoshan and Dashiqiao. The 2.0 – 1.8 Ga rocks are widely distributed in the khondalite belt of the Inner Mongolia Suture Zone (Santosh, 2010), several complexes within the TNCO, and the Paleoproterozoic *meta*-volcano-sedimentary complex (i.e., Liaohe Group) in the Liaoning Province (Li et al., 2018; Tang and Santosh, 2018a; Zhao et al., 2005). (2) A large number of granites with ages ranging from 2.2 to 1.90 Ga were emplaced into the Inner Mongolia–Eastern Hebei Orogenic Belt (Kusky and Li, 2003). (3) Several ~ 2.0 Ga granite intrusions are recognized in the Tianzheng, and the Lüliang Mountains, and voluminous S-type granites were generated through anatexis and metamorphism of the khondalites in the western part of the North China Craton (Kusky and Li, 2003). (4) Several ~ 2.2 Ga magnesian andesites, Nb-enriched basalt-andesites, and adakitic rocks are also identified in the Lüliang Complex and represent a Paleoproterozoic subduction belt in the North China Craton (Liu et al., 2014). (5) Most of these Paleoproterozoic magmatic rocks also show zircon grains with high and positive $\varepsilon_{Hf}(t)$ values (Fig. 10), which are identical to those of the 2.2–1.9 Ga detrital zircons of the Changcheng Group (Li et al., 2018; Liu et al., 2014; Tang and Santosh, 2018a).

5.3. Episodic Neoarchean-Paleoproterozoic crust growth of the North China Craton

The high $\varepsilon_{Hf}(t)$ values from zircon grains are commonly considered to be representative of juvenile continental materials (Jahn, 2004; Kemp et al., 2007, 2005). The detrital zircons of the Changcheng Group have high and positive $\varepsilon_{Hf}(t)$ values (+0.1–+34.6; Fig. 10). Compared with their crystallization ages, these Neoarchean to Paleoproterozoic zircons have relatively young T_{2DM} ages of 2.0–2.9 Ga. Thus, we infer two major crust growth events in NCC at 2.7–2.5 Ga and 2.2–1.9 Ga. The former could be subdivided into two phases at 2.75–2.60 Ga and ~ 2.5 Ga. The first phase of 2.75–2.60 Ga crust growth is dominated by the plume-arc interaction process (Guo et al., 2016; Li et al., 2016; Santosh et al., 2017; Tang and Santosh, 2018a), and involved both vertical (mantle plume) and/or lateral (in convergent margins) accretion. The second phase of ~ 2.5 Ga crust growth involves oceanic lithospheric subduction (Li et al., 2016; Santosh et al., 2016, 2017) and is dominated by lateral accretion. The latter 2.2 – 1.9 Ga crust growth events also could be subdivided into two phases at 2.20 – 2.00 Ga and 2.00 – 1.90 Ga. The first event at 2.20 – 2.0 Ga is related to the oceanic subduction and the collision between the Eastern and Western Blocks (Liu et al., 2014; Tang and Santosh, 2018a; Zhou et al., 2017), and dominated by lateral accretion. The second event at 2.0–1.90 Ga occurred possibly during the post-collisional extension setting, and could be ascribed to vertical (intraplate setting) accretion.

Furthermore, late Paleoproterozoic (1.71 – 1.62 Ga) volcanic and intrusive rocks are also identified in the Changcheng Group, and are widely reported in the NCC (Liu et al., 2016; Lu et al., 2002; Sun et al., 2017; Wang et al., 2013, 2015; Xia et al., 2013). As shown in Fig. 10, these rocks also show high and positive $\varepsilon_{Hf}(t)$ values for zircon grains. Thus, we propose that the NCC might have experienced a late Paleoproterozoic (1.71 – 1.62 Ga) crust growth event. The generation of these magmatic rocks was believed to be triggered by the delamination of the continental lithosphere in a post-orogenic setting following the final amalgamation of the North China Craton within the Columbia supercontinent (Wang et al., 2015). Thus, the late Paleoproterozoic (1.71 – 1.62 Ga) crustal growth event could also be ascribed to vertical (in intraplate setting) accretion.

In summary, the NCC has experienced three phase of Neoarchean-Paleoproterozoic crust growth at 2.7 – 2.5 Ga, 2.2 – 1.9 Ga and 1.7 – 1.6 Ga, which involved both vertical (mantle plume) and/or lateral (convergent margin) accretions.

6. Conclusions

(1). Detrital zircon grains from the Changcheng Group define two major age populations at 2.7 – 2.5 Ga and 2.2 – 1.9 Ga, with high and positive $\varepsilon_{Hf}(t)$ values of + 0.1 to + 34.6.
(2). Both the 2.7 – 2.5 Ga and 2.2 – 1.9 Ga detrital zircons were derived from the NCC basement rocks.
(3). The NCC experienced three phases of Neoarchean-Paleoproterozoic crust growth at 2.7 – 2.5 Ga, 2.2 – 1.9 Ga and 1.7 – 1.6 Ga, involving both vertical (mantle plume) and/or lateral (convergent margins) accretions.

CRediT authorship contribution statement

Xiaoping Liu: Conceptualization, Funding acquisition, Investigation. **Huichuan Liu:** Investigation, Data curation. **Pin Gao:** Data curation. **Wenqi Li:** . **Huan Liu:** Investigation, Validation. **Jiakai Hou:** Investigation, Validation.

Declaration of Competing Interest

The authors declare that they have no known competing financial interests or personal relationships that could have appeared to influence the work reported in this paper.

Acknowledgements

We would like to thank Jianwei Xiao and Tingting Zhang for helping with the fieldwork and zircon U-Pb analyses. We are grateful for the constructive comments by Associate Editor Yongjiang Liu and two anonymous reviewers. We thank Prof. M. Santosh for several discussions, guidance, and valuable input for manuscript corrections. The study is funded by the Science Foundation of China University of Petroleum, Beijing (2462018YJRC030 and 2462020YXZZ020) and the National Natural Science Foundation of China (Grant No. 42072150).

Appendix A. Supplementary material

Supplementary data to this article can be found online at https://doi.org/10.1016/j.gr.2021.04.001.

References

Allegre, C.J., Othman, D.B., 1980. Nd-Sr isotopic relationship in granitoid rocks and continental-crust development – a chemical approach to orogenesis. Nature 286 (5771), 335–342.

Cawood, P.A., Hawkesworth, C.J., 2019. Continental crustal volume, thickness and area, and their geodynamic implications. Gondwana Res. 66, 116–125.

Chen, N., Liao, F., Wang, L.u., Santosh, M., Sun, M., Wang, Q., Mustafa, H.A., 2013. Late Paleoproterozoic multiple metamorphic events in the Quanji Massif: Links with Tarim and North China Cratons and implications for assembly of the Columbia supercontinent. Precambr. Res. 228, 102–116.

Darbyshire, D.P.F., Shepherd, T.J., 1994. Nd and Sr Isotope Constraints on the Origin of the Cornubian Batholith, Sw England. Journal of the Geological Society 151 (5), 795–802.

Dhuime, B., Hawkesworth, C., Cawood, P., 2011. When continents formed. Science 331, 154–155.

Furnes, H., Dilek, Y., Zhao, G., Safonova, I., Santosh, M., 2020. Geochemical characterization of ophiolites in the Alpine-Himalayan Orogenic Belt: Magmatically and tectonically diverse evolution of the Mesozoic Neotethyan oceanic crust. Earth Sci. Rev. 208, 103258.

Gao, P., Santosh, M., 2020. Mesoarchean accretionary mélange and tectonic erosion in the Archean Dharwar Craton, southern India: Plate tectonics in the early Earth. Gondwana Res. 85, 291–305.

Gao, W., Zhang, C.H., Gao, L.Z., Shi, X.Y., Liu, Y.M., Song, B., 2008. Zircon SHRIMP U-Pb Age of Rapakivi Granite in Miyun, Beijing, China and its Tectono-Stratigraphic Implications. Geological Bulletin of China 27 (6), 793–798.

Geng, H.Y., Sun, M., Yuan, C., Xiao, W.J., Xian, W.S., Zhao, G.C., Zhang, L.F., Wong, K., Wu, F.Y., 2009. Geochemical, Sr-Nd and zircon U-Pb-Hf isotopic studies of Late Carboniferous magmatism in the West Junggar, Xinjiang: Implications for ridge subduction?. Chem. Geol. 266 (3–4), 364–389.

Griffin, W.L., Belousova, E.A., Shee, S.R., Pearson, N.J., O'Reilly, S.Y., 2004. Archean crustal evolution in the northern Yilgarn Craton: U-Pb and Hf-isotope evidence from detrital zircons. Precambr. Res. 131 (3–4), 231–282.

Griffin, W.L., Wang, X., Jackson, S.E., Pearson, N.J., O'Reilly, S.Y., Xu, X.S., Zhou, X. M., 2002. Zircon chemistry and magma mixing, SE China: In-situ analysis of Hf isotopes. Tonglu and Pingtan igneous complexes. Lithos 61 (3–4), 237–269.

Guo, R.R., Liu, S.W., Santosh, M., Li, Q.G., Bai, X., Wang, W., 2013. Geochemistry, zircon U-Pb geochronology and Lu-Hf isotopes of metavolcanics from eastern Hebei reveal Neoarchean subduction tectonics in the North China Craton. Gondwana Res. 24 (2), 664–686.

Guo, X.F., Wang, Y.J., Liu, H.C., Zi, J.W., 2016. Zircon U-Pb. Geochronology of the Cenozoic Granitic Mylonite along the Ailaoshan-Red River Shear Zone: New Constraints on the Timing of the Sinistral Shearing. J. Earth Sci. 27 (3), 435–443.

Hawkesworth, C.J., Kemp, A.I.S., 2006. Using hafnium and oxygen isotopes in zircons to unravel the record of crustal evolution. Chem. Geol. 226 (3–4), 144–162.

Hawkesworth, C., Cawood, P.A., Dhuime, B., 2019. Rates of generation and growth of the continental crust. Geosci. Front. 10 (1), 165–173.

Hu, Z.C., Liu, Y.S., Gao, S., Liu, W., Yang, L., Zhang, W., Tong, X., Lin, L., Zong, K.Q., Li, M., Chen, H., Zhou, L., 2012. Improved in situ Hf isotope ratio analysis of zircon using newly designed X skimmer cone and Jet sample cone in combination with the addition of nitrogen by laser ablation multiple collector ICP-MS. J. Anal. At. Spectrom. 27, 1391–1399.

Hu, Z.C., Zhang, W., Liu, Y.S., Gao, S., Li, M., Zong, K.Q., Chen, H.H., Hu, S.H., 2015. "Wave" signal-smoothing and mercury-removing device for laser ablation quadrupole and multiple collector ICPMS analysis: application to lead isotope analysis. Anal. Chem. 87 (2), 1152–1157.

Jahn, B.M., 2004. Granitoids of the Central Asian Orogenic Belt and continental growth in the Phanerozoic. Geological Society, London, Special Publications 226, 73–100.

Jayananda, M., Aadhiseshan, K.R., Kusiak, M.A., Wilde, S.A., Sekhamo, K.U., Guitreau, M., Santosh, M., Gireesh, R.V., 2020. Multi-stage crustal growth and Neoarchean geodynamics in the Eastern Dharwar Craton, southern India. Gondwana Res. 78, 228–260.

Kemp, A.I.S., Foster, G.L., Schersten, A., Whitehouse, M.J., Darling, J., Storey, C., 2009. Concurrent Pb-Hf isotope analysis of zircon by laser ablation multi-collector ICP-MS, with implications for the crustal evolution of Greenland and the Himalayas. Chem. Geol. 261 (3–4), 244–260.

Kemp, A.I.S., Hawkesworth, C.J., Foster, G.L., Paterson, B.A., Woodhead, J.D., Hergt, J. M., Gray, C.M., Whitehouse, M.J., 2007. Magmatic and crustal differentiation history of granitic rocks from Hf-O isotopes in zircon. Science 315 (5814), 980–983.

Kemp, A.I.S., Wilde, S.A., Hawkesworth, C.J., Coath, C.D., Nemchin, A., Pidgeon, R.T., Vervoort, J.D., DuFrane, S.A., 2010. Hadean crustal evolution revisited: New constraints from Pb-Hf isotope systematics of the Jack Hills zircons. Earth Planet. Sci. Lett. 296 (1–2), 45–56.

Kemp, A.I.S., Wormald, R.J., Whitehouse, M.J., Price, R.C., 2005. Hf isotopes in zircon reveal contrasting sources and crystallization histories for alkaline to peralkaline granites of Temora, southeastern Australia. Geology 33 (10), 797–800.

Kusky, T.M., Li, J.H., 2003. Paleoproterozoic tectonic evolution of the North China Craton. J. Asian Earth Sci. 22 (4), 383–397.

Lamb, D.M., Awramik, S.M., Chapman, D.J., Zhu, S., 2009. Evidence for eukaryotic diversification in the similar to 1800 million-year-old Changzhougou Formation. North China. Precambrian Research 173 (1–4), 93–104.

Li, C., Planavsky, N.J., Love, G.D., Reinhard, C.T., Hardisty, D., Feng, L.J., Bates, S.M., Huang, J., Zhang, Q.R., Chu, X.L., Lyons, T.W., 2015. Marine redox conditions in the middle Proterozoic ocean and isotopic constraints on authigenic carbonate formation: Insights from the Chuanlinggou Formation, Yanshan Basin, North China. Geochim. Cosmochim. Acta 150, 90–105.

Li, H.K., Li, H.M., Lu, S.N., 1995. Grain zircon U-Pb ages for volcanic rocks from Tuanshanzi Formation of Changcheng System and Their Geological impliacations. Geochimica 24 (1), 43–48 (In Chinese with English Abstract).

Li, H.K., Su, W.B., Zhou, H.Y., Geng, J.Z., Xiang, Z.Q., Cui, Y.R., Liu, W.C., Lu, S.N., 2011. The base age of the Changchengian System at the northern North China Craton should be younger than 1670 Ma: Constraints from zircon U-Pb LA-MC-ICPMS dating of a granite-porphyry dike in Miyun County, Beijing. Earth Science Frontiers 18, 108–120 (In Chinese with English abstract).

Li, H.K., Zhu, S.X., Xiang, Z.Q., Su, W., Lu, S.N., Zhou, H.Y., Geng, J., Li, S., Yang, F.J., 2010. Zircon U-Pb Dating On Tuff Bed from Gaoyuzhuang Formation in Yanqing, Beijing: Further Constraints on the New Subdivision of the Mesoproterozoic Stratigraphy in the Northern North China Craton. Acta Petrologica Sinica 07, 2131–2140 (In Chinese with English abstract).

Li, H.K., Lu, S.N., Su, W.B., Xiang, Z.Q., Zhou, H.Y., Zhang, Y.Q., 2013. Recent advances in the study of the Mesoproterozoic Geochronology in the North China Craton. Journal of Asian Earth Sci. 72 (SI), 216–227.

Li, S.S., Santosh, M., Cen, K., Teng, X.M., He, X.F., 2016. Neoarchean convergent margin tectonics associated with microblock amalgamation in the North China Craton: Evidence from the Yishui Complex. Gondwana Res. 38, 113–131.

Li, W., Dong, Y.P., Liu, X.M., 2018. Geochronology, geochemistry and Nd-Hf isotopes of the Xiaokouzi granite from the Helanshan complex: Constraints on the Paleoproterozoic evolution of the Khondalite Belt, North China Craton. Precambr. Res. 317, 57–76.

Liew, T.C., Hofmann, A.W., 1988. Precambrian Crustal Components, Plutonic Associations, Plate Environment of the Hercynian Fold Belt of Central-Europe - Indications from a Nd and Sr Isotopic Study. Contrib. Miner. Petrol. 98 (2), 129–138.

Liu, C.H., Zhao, G.C., Liu, F.L., Shi, J.R., 2014. 2.2 Ga magnesian andesites, Nb-enriched basalt-andesites, and adakitic rocks in the Luliang Complex: Evidence for early Paleoproterozoic subduction in the North China Craton. Lithos 208, 104–117.

Liu, J.F., Li, J.Y., Qu, J.F., Hu, Z.C., Feng, Q.W., Guo, C.L., 2016. Late Paleoproterozoic tectonic setting of the northern margin of the North China Craton: Constraints from the geochronology and geochemistry of the mangerites in the Longhua and Jianping areas. Precambr. Res. 272, 57–77.

Liu, X.G., Zhang, J., Li, S.Z., Li, X.Y., Yin, C.Q., 2019. Tectono-sedimentary evolution of the Mesoproterozoic basins in the southern Yan-Liao and Mianchi-Queshan areas: insights from stratigraphic pattern and detrital zircon geochronology. Int. J. Earth Sci. 109, 43–62.

Liu, Y.S., Hu, Z.C., Gao, S., Günther, D., Xu, J., Gao, C.G., Chen, H.H., 2008. In situ analysis of major and trace elements of anhydrous minerals by LA-ICP-MS without applying an internal standard. Chem. Geol. 257 (1–2), 34–43.

Liu, Y.S., Gao, S., Hu, Z.C., Gao, C.G., Zong, K.Q., Wang, D.B., 2010. Continental and oceanic crust recycling-induced melt-peridotite interactions in the Trans-North China Orogen: U-Pb dating, Hf isotopes and trace elements in zircons of mantle xenoliths. J. Petrol. 51 (1–2), 537–571.

Lu, S.N., Li, H.M., 1991. A precise U-Pb single zircon age determination for the volcanics of the Dahongyu Formation, Changcheng System in Jinxian. Bulletin of the Chinese Academy of Geological Sciences 22, 137–145 (in Chinese with English abstract).

Lu, S.N., Yang, C.L., Li, H.K., Li, H.M., 2002. A group of rifting events in the terminal paleoproterozoic in the North China craton. Gondwana Res. 5 (1), 123–131.

Lu, S.N., Zhao, G.C., Wang, H.C., Hao, G.J., 2008. Precambrian metamorphic basement and sedimentary cover of the North China Craton: A review. Precambr. Res. 160 (1–2), 77–93.

Ludwig, K.R., 2003. ISOPLOT 3.00: A Geochronological Toolkit for Microsoft Excel. Berkeley Geochronology Center, California, Berkeley, 39.

Meert, J.G., 2012. What's in a name? The Columbia (Paleopangaea/Nuna) supercontinent. Gondwana Res. 21, 987–993.

Meert, J.G., Santosh, M., 2017. The Columbia supercontinent revisited. Gondwana Res. 50, 76–83.

Meng, Q.R., Wei, H.H., Qu, Y.Q., Ma, S.X., 2011. Stratigraphic and sedimentary records of the rift to drift evolution of the northern North China craton at the Paleo- to Mesoproterozoic transition. Gondwana Res. 20 (1), 205–218.

Miao, L.Y., Moczydlowska, M., Zhu, S.X., Zhu, M.Y., 2019. New record of organic-walled, morphologically distinct microfossils from the late Paleoproterozoic Changcheng Group in the Yanshan Range, North China. Precambr. Res. 321, 172–198.

Palin, R.M., Santosh, M., 2020. Plate tectonics: What, where, why, and when?. Gondwana Res. https://doi.org/10.1016/j.gr.2020.11.001.

Palin, R.M., Santosh, M., Cao, W.T., Li, S.S., Hernández-Uribe, D., Parsons, A., 2020. Secular change and the onset of plate tectonics on Earth. Earth Sci. Rev. 207, 103172.

Peng, P., Liu, F., Zhai, M.G., Guo, J.H., 2012a. Age of the Miyun dike swarm: Constraints on the maximum depositional age of the Changcheng System. Chin. Sci. Bull. 57 (1), 105–110 (in Chinese with English abstract).

Peng, T.P., Fan, W.M., Peng, B.X., 2012b. Geochronology and geochemistry of late Archean adakitic plutons from the Taishan granite-greenstone Terrain: Implications for tectonic evolution of the eastern North China Craton. Precambr. Res. 208, 53–71.

Peng, Y.B., Bao, H.M., Yuan, X.L., 2009. New morphological observations for Paleoproterozoic acritarchs from the Chuanlinggou Formation. North China. Precambrian Research 168 (3–4), 223–232.
Qu, Y.Q., Pan, J.G., Ma, S.X., Lei, Z.P., Li, L., Wu, G.L., 2014. Geological characteristics and tectonic significance of unconformities in Mesoproterozoic successions in the northern margin of the North China Block. Geosci. Front. 5 (1), 127–138.
Santosh, M., 2013. Evolution of continents, cratons and supercontinents: building the habitable Earth. Curr. Sci. 104 (7), 871–879.
Santosh, M., 2010. Assembling North China Craton within the Columbia supercontinent: The role of double-sided subduction. Precambr. Res. 178 (1–4), 149–167.
Santosh, M., Teng, X.M., He, X.F., Tang, L., Yang, Q.Y., 2016. Discovery of Neoarchean suprasubduction zone ophiolite suite from Yishui Complex in the North China Craton. Gondwana Res. 38, 1–27.
Santosh, M., Tsunogae, T., Yang, C.X., Han, Y.S., Hari, K.R., Prasanth, M.M., Uthup, S., 2020a. The Bastar craton, central India: A window to Archean-Paleoproterozoic crustal evolution. Gondwana Res. 79, 157–184.
Santosh, M., Gao, P., Yu, B., Yang, C.X., Kwon, S.H., 2020b. Neoarchean suprasubduction zone ophiolite discovered from the Miyun Complex: Implications for Archean-Paleoproterozoic Wilson cycle in the North China Craton. Precambr. Res. 342, 105710.
Santosh, M., Teng, X.M., He, X.F., Tang, L., Yang, Q.Y., 2017. Discovery of Neoarchean suprasubduction zone ophiolite suite from Yishui Complex in the North China Craton. Gondwana Res. 48, 311.
Shi, K.X., Wang, C.M., Santosh, M., Du, B., Yang, L.F., Chen, Q., 2019. New insights into Neoarchean-Paleoproterozoic crustal evolution in the North China Craton: Evidence from zircon U-Pb geochronology, Lu-Hf isotopes and geochemistry of TTGs and greenstones from the Luxi Terrane. Precambr. Res. 327, 232–254.
Shi, Y.R., Wilde, S.A., Zhao, X.T., Ma, Y.S., Du, L.L., Liu, D.Y., 2012. Late Neoarchean magmatic and subsequent metamorphic events in the northern North China Craton: SHRIMP zircon dating and Hf isotopes of Archean rocks from Yunmengshan Geopark, Miyun. Beijing. Gondwana Research 21 (4), 785–800.
Soderlund, Ulf, Patchett, Jonathan P., Vervoort, Jeffrey D., Isachsen, Clark E., 2004. The Lu-176 decay constant determined by Lu–Hf and U–Pb isotope systematics of Precambrian mafic intrusions. Earth and Planetary Science Letters 219, 311–324.
Sun, Z.J., Yu, H.N., Li, C., Xue, H.Y., Zhang, H.F., 2017. Paleoproterozoic (ca. 1.7 Ga) magmatism in Chifeng, Inner Mongolia: implications for the tectonic evolution of the Trans-North China Orogen. Arabian J. Geosci. 10 (20), 453–467.
Tang, G.J., Wang, Q., Wyman, D.A., Li, Z.X., Xu, Y.G., Zhao, Z.H., 2012a. Recycling oceanic crust for continental crustal growth: Sr-Nd-Hf isotope evidence from granitoids in the western Junggar region, NW China. Lithos 128, 73–83.
Tang, G.J., Wang, Q., Wyman, D.A., Li, Z.X., Zhao, Z.H., Yang, Y.H., 2012b. Late Carboniferous high epsilon(Nd)(t)-epsilon(Hf)(t) granitoids, enclaves and dikes in western Junggar, NW China: Ridge-subduction-related magmatism and crustal growth. Lithos 140, 86–102.
Tang, G.J., Wyman, D.A., Wang, Q., Li, J., Li, Z.X., Zhao, Z.H., Sun, W.D., 2012c. Asthenosphere-lithosphere interaction triggered by a slab window during ridge subduction: Trace element and Sr-Nd-Hf-Os isotopic evidence from Late Carboniferous tholeiites in the western Junggar area (NW China). Earth Planet. Sci. Lett. 329, 84–96.
Tang, L., Santosh, M., 2018a. Neoarchean-Paleoproterozoic terrane assembly and Wilson cycle in the North China Craton: an overview from the central segment of the Trans North China Orogen. Earth Sci. Rev. 182, 1–27.
Tang, L., Santosh, M., 2018b. Neoarchean granite-greenstone belts and related ore mineralization in the North China Craton: An overview. Geosci. Front. 9 (3), 751–768.
Tian, Z., Xiao, W., 2020. An Andean-type arc transferred into a Japanese-type arc at final closure stage of the Palaeo-Asian Ocean in the southernmost of Altaïds. Geol. J. 55 (3), 2023–2043.
Tian, H., Zhang, J., Li, H.K., Su, W.B., Zhou, H.Y., Yang, L.G., Xiang, Z.Q., Geng, J.Z., Liu, H., Zhu, S.X., Xu, Z.Q., 2015. Zircon LA-MC-ICPMS U-Pb Dating of Tuff from Mesoproterozoic Gaoyuzhuang Formation in Jixian County of North China and its Geological Significance. Acta Geoscientica Sinica 5, 647–658 (in Chinese with English abstract).
Wan, Y.S., Liu, D.Y., Wang, W., Song, T.R., Kroner, A., Dong, C.Y., Zhou, H.Y., Yin, X.Y., 2011. Provenance of Meso- to Neoproterozoic cover sediments at the Ming Tombs, Beijing, North China Craton: An integrated study of U-Pb dating and Hf isotopic measurement of detrital zircons and whole-rock geochemistry. Gondwana Res. 20 (1), 219–242.
Wan, Y.S., Zhang, Q.D., Song, T.R., 2003. SHRIMP ages of detrital zircons from the Changcheng System in the Ming Tombs area, Beijing: Constraints on the protolith nature and maximum depositional age of the Mesoproterozoic cover of the North China Craton. Chin. Sci. Bull. 48 (22), 2500–2506.
Wang, W., Cawood, P.A., Liu, S.W., Guo, R.R., Bai, X., Wang, K., 2017. Cyclic formation and stabilization of Archean lithosphere by accretionary orogenesis: Constraints from TTG and potassic granitoids. North China Craton. Tectonics 36 (9), 1724–1742.
Wang, W., Cawood, P.A., Liu, S.W., Guo, R.R., Bai, X., Wang, K., 2013. Geochemistry and zircon U-Pb-Hf isotopes of the late Paleoproterozoic Jianping diorite-monzonite-syenite suite of the North China Craton: Implications for petrogenesis and geodynamic setting. Lithos 162, 175–194.
Wang, W., Liu, S.W., Santosh, M., Deng, Z.B., Guo, B.R., Zhao, Y., Zhang, S.H., Yang, P. T., Bai, X., Guo, R.R., 2015. Late Paleoproterozoic geodynamics of the North China Craton: Geochemical and zircon U-Pb-Hf records from a volcanic suite in the Yanliao rift. Gondwana Res. 27 (1), 300–325.
Wu, K.K., Zhao, G.C., Sun, M., Yin, C.Q., He, Y.H., Tam, P.Y., 2013. Metamorphism of the northern Liaoning Complex: Implications for the tectonic evolution of Neoarchean basement of the Eastern Block. North China Craton. Geoscience Frontiers 4 (3), 305–320.
Wu, M.L., Lin, S.F., Wan, Y.S., Gao, J.F., 2016. Crustal evolution of the Eastern Block in the North China Craton: Constraints from zircon U-Pb geochronology and Lu-Hf isotopes of the Northern Liaoning Complex. Precambr. Res. 275, 35–47.
Xia, L.Q., Xia, Z.C., Xu, X.Y., Li, X.M., Ma, Z.P., 2013. Late Paleoproterozoic rift-related magmatic rocks in the North China Craton: Geological records of rifting in the Columbia supercontinent. Earth Sci. Rev. 125, 69–86.
Yang, J.H., Wu, F.Y., Liu, X.M., Xie, L.W., 2005. Zircon U-Pb Ages and Hf Isotopes and their Geological Significance of the Miyun Rapakive Granites from Beijing, China. Acta Petrologica Sinica 06, 1633–1644 (in Chinese with English abstract).
Zhai, M.G., Santosh, M., 2011. The early Precambrian odyssey of the North China Craton: A synoptic overview. Gondwana Res. 20 (1), 6–25.
Zhai, M.G., Santosh, M., 2013. Metallogeny of the North China Craton: Link with secular changes in the evolving Earth. Gondwana Res. 24 (1), 275–297.
Zhang, J., Tian, H., Li, H.K., Su, W.B., Zhou, H.Y., Xiang, Z.Q., Geng, J.Z., Yang, L.G., 2015. Age, geochemistry and zircon Hf isotope of the alkaline basaltic rocks in the middle section of the Yan-Liao aulacogen along the northern margin of the North China Craton: New evidence for the breakup of the Columbia Supercontinent. Acta Petrologica Sinica 31 (10), 3129–3146 (In Chinese with English Abstract).
Zhang, S.H., Zhao, Y., Ye, H., Hu, J.M., Wu, F., 2013. New Constraints on Ages of the Chuanlinggou and Tuanshanzi Formations of the Changcheng System in the Yan-Liao Area in the Northern North China Craton. Acta Petrologica Sinica 29 (07), 2481–2490 (in Chinese with English abstract).
Zhao, G.C., Cawood, P.A., Li, S.Z., Wilde, S.A., Sun, M., Zhang, J., He, Y.H., Yin, C.Q., 2012. Amalgamation of the North China Craton: Key issues and discussion. Precambr. Res. 222, 55–76.
Zhao, G.C., Sun, M., Wilde, S.A., Li, S.Z., 2005. Late Archean to Paleoproterozoic evolution of the North China Craton: key issues revisited. Precambr. Res. 136 (2), 177–202.
Zhao, G.C., Zhai, M.G., 2013. Lithotectonic elements of Precambrian basement in the North China Craton: Review and tectonic implications. Gondwana Res. 23 (4), 1207–1240.
Zhong, Y.T., He, C., Chen, N.S., Xia, B., Zhou, Z.Q., Chen, B.H., Wang, G.Q., 2018. Tectonothermal Records in Migmatite-Like Rocks of the Guandi Complex in Zhoukoudian, Beijing: Implications for Late Neoarchean to Proterozoic Tectonics of the North China Craton. J. Earth Sci. 29 (5), 1254–1275.
Zhou, L.G., Zhai, M.G., Lu, J.S., Zhao, L., Wang, H.Z., Wu, J.L., Liu, B., Zou, Y., Shan, H.X., Cui, X.H., 2017. Paleoproterozoic metamorphism of high-grade granulite facies rocks in the North China Craton: Study advances, questions and new issues. Precambr. Res. 303, 520–547.
Zhou, Y.Y., Zhao, T.P., Zhai, M.G., Gao, J.F., Sun, Q.Y., 2014. Petrogenesis of the Archean tonalite-trondhjemite-granodiorite (TTG) and granites in the Lushan area, southern margin of the North China Craton: Implications for crustal accretion and transformation. Precambr. Res. 255, 514–537.
Zong, K.Q., Klemd, R., Yuan, Y., He, Z.Y., Guo, J.L., Shi, X.L., Liu, Y.S., Hu, Z.C., Zhang, Z. M., 2017. The assembly of Rodinia: The correlation of early Neoproterozoic (ca. 900 Ma) high-grade metamorphism and continental arc formation in the southern Beishan Orogen, southern Central Asian Orogenic Belt (CAOB). Precambr. Res. 290, 32–48.